Thin Solid Films xxx (2014) xxx–xxx

Contents lists available at ScienceDirect

Thin Solid Films

journal homepage: www.elsevier.com/locate/tsf

Up-conversion effect of Er- and Yb-doped ZnO thin films

M. Lluscà [a,*], J. López-Vidrier [b], A. Antony [a,c], S. Hernández [b], B. Garrido [b], J. Bertomeu [a]

[a] Department of Applied Physics and Optics, Universitat de Barcelona, Barcelona 08028, Spain
[b] Department of Electronics, Universitat de Barcelona, Barcelona 08028, Spain
[c] Indian Institute of Technology Bombay, 400076 Mumbai, India

ARTICLE INFO

Article history:
Received 25 July 2013
Received in revised form 21 March 2014
Accepted 21 March 2014
Available online xxxx

Keywords:
Up-conversion
Erbium
Ytterbium
ZInc Oxide
Photoluminescence

ABSTRACT

Visible up-conversion in ZnO:Er and ZnO:Er:Yb thin films deposited by RF magnetron sputtering under different O_2-rich atmospheres has been studied. Conventional photoluminescence (325 nm laser source) and up-conversion (980 nm laser source) have been performed in the films before and after an annealing process at 800 °C. The resulting spectra demonstrate that the thermal treatment, either during or post-deposition, activates optically the Er^{3+} ions, being the latter process much more efficient. Moreover, the atmosphere during deposition was also found to be an important parameter, as the deposition under O_2 flow increases the optical activity of Er^{+3} ions. In addition, the inclusion of Yb^{3+} ions into the films has shown an enhancement of the visible up-conversion emission at 660 nm by a factor of 4, which could be associated to either a better energy transfer from the $^2F_{5/2}$ Yb level to the $^4I_{11/2}$ Er one, or to the prevention of having Er_2O_3 clustering in the films.

1. Introduction

Rare earth (RE) materials have been widely studied due to their optical emission, which occurs as a result of intra 4*f*–4*f* shell transitions [1]. Fiber lasers and amplifiers, plasma displays, fluorescent lamps, bioimaging and solar cells are just a few applications that take advantage of their optical properties [2–4]. In particular, Er is mostly used as a dopant thanks to its high photoemission at 1.5 μm and its capability of up-converting light from the infrared (IR) to the visible range. Actually, Er doping creates intermediate states within the band gap characterized by long lifetimes [5]. However, the small cross-section of Er^{3+} ions makes this emission process difficult, obtaining an inefficient up-conversion process. In order to enhance the Er up-conversion efficiency, Er-doped systems can be co-doped with Yb^{3+} ions, as reported in similar systems [6–9]. Er and Yb have the capability to cooperate together to convert IR light into visible light because of the matching of their energy levels for $\lambda = 980$ nm (see Fig. 1).

The host materials commonly used in the reported works of up-conversion from Er and Yb are phosphate and chalcogenide glasses, as well as $NaYF_4$ nanoparticles [7–9]. Besides, SiO_2 and TiO_2 host matrices are promising for wave guiding and amplification applications [10–12]. In this work, ZnO has been chosen as a host matrix, because its wide band gap energy of 3.4 eV [13] can be used for the excitation of both Er and Yb species. It has been demonstrated that Er acts as an optically active center if it is surrounded by oxygen (ErO_6) forming a pseudo-octahedron structure with a C_{4v} symmetry that can allow the 4*f*–4*f* transitions to occur [14]. That means that Er replacing Zn in the ZnO matrix forms ErO_4 and does not act as an optically active center; therefore an annealing treatment is required to change Er local structure, forming ErO_6 clusters either in the ZnO matrix or at the grain boundaries [15,16].

Three different ZnO-based thin films were deposited by means of magnetron sputtering onto Corning 1737F glass substrates. ZnO layers were doped with Er or co-doped with Er and Yb under different deposition conditions. All the layers were annealed after deposition to change the local surrounding of Er. The role of oxygen during deposition in the conventional and up-conversion photoluminescence, as well as the strong enhancement of the up-conversion emission by Yb co-doping, was investigated.

2. Experimental details

ZnO:Er and ZnO:Er:Yb thin films were grown on Corning 1737F glass substrates by a RF magnetron sputtering ATC-ORION 8 HV from AJA International, Inc. ZnO target with 99.995% purity and a diameter of 3 in. was used for the deposition. Er and Yb doping was achieved by placing small pellets of Er_2O_3 or both Er_2O_3 and Yb_2O_3 on the erosion area of the target surface. The pellets (13 mm diameter) were made by pressing Er_2O_3 and Yb_2O_3 powders of 99.99% purity with a Specac Hydraulic Press, and the as-prepared pellets were annealed in O_2 flow at 800 °C for 4 h in a quartz tubular furnace.

Three different ZnO films were deposited at a working pressure of 0.4 Pa in Ar gas, while the substrate rotation was kept at 10 rpm and the target to substrate distance was 12 cm. The first two samples, EZO

* Corresponding author at: Department of Applied Physics and Optics Universitat de Barcelona c/Martí i Franquès, 1 08028 Barcelona, Spain. Tel.: +34 93 40 39223.
E-mail address: marta.llusca@ub.edu (M. Lluscà).

http://dx.doi.org/10.1016/j.tsf.2014.03.078
0040-6090/

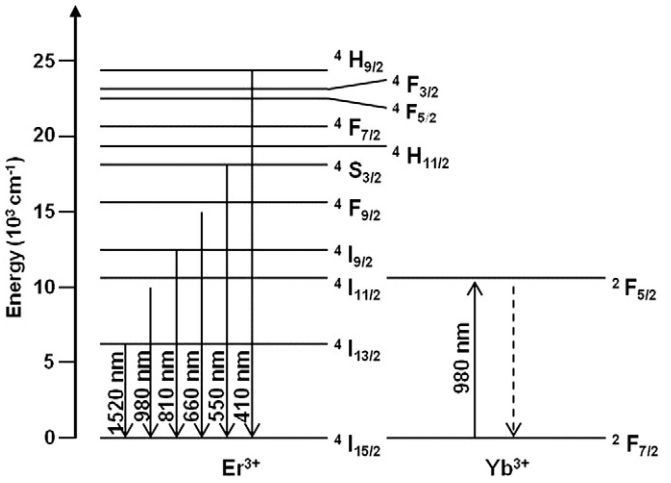

Fig. 1. Generic representation of the energy levels diagram of Er^{3+} and Yb^{3+} ions.

(ZnO doped with Er) and EYZO (ZnO doped with Er and Yb) were deposited at room temperature (RT) without any intentional heating of the substrate at an RF power of 120 W. The deposition rate for these samples was 2.4 nm/min and the thickness of the samples was 800 nm. The third sample, OEYZO, was doped with Er and Yb but deposited at a lower RF power (60 W) and at a substrate temperature of 350 °C in oxygen presence (oxygen-to-argon ratio of 1:4), with the aim to favor the incorporation of oxygen into the growing film. A lower rf power was used to have a slow growth rate to enhance oxygen incorporation and to yield better stoichiometric film. This sample had a thickness of 450 nm and the deposition rate was 0.8 nm/min. The three samples EZO, EYZO and OEYZO have been annealed at 800 °C for 1 h in a quartz tubular furnace, and are labeled as EZOA, EYZOA and OEYZOA, respectively.

The structure, composition and optical properties have been studied before and after the thermal annealing. The crystalline nature of the films was analyzed using the X-ray diffraction (XRD) technique (PANalytical X'Pert PRO MPD Alpha1 powder system, using Cu K_α radiation, $\lambda = 1.5406$ Å). The instrumental broadening correction has been applied to calculate the integral breadth. The average crystallite size $\langle D \rangle$ (volume-weighted domain size in the direction normal to the diffracting lattice planes) of the films can be estimated from the integral breadth (β) deduced from the pseudo-Voigt peak profile fitting of the XRD pattern by using the following equation [17]:

$$\langle D \rangle = \frac{\lambda}{\beta \cos\theta} \quad (1)$$

where β is the integral breadth, λ is the X-ray wavelength, and θ is the Bragg's diffraction angle corresponding to the diffraction peak.

X-ray Photoelectron Spectroscopy (XPS) analysis was performed using a PHI 5500 Multitechnique System (from Physical Electronics) with a monochromatic X-ray source (Al K_α line, with an energy of 1486.6 eV and at a power of 350 W) placed perpendicular to the analyzer axis and calibrated using the $^3d_{5/2}$ line of Ag with a full-width at half-maximum (FWHM) of 0.8 eV. XPS spectra were recorded after sputtering the sample surface with an Ar^+ ion source (4 keV energy). The composition was calculated from the integrated peak areas of the spectra and a Shirley background subtraction was carried out before proceeding to analyze the chemical composition of the films. The position of the Ar 2*p* peak that appeared after sputtering the surface was used to correct any eventual shift due to charge effects.

The optical transmittance spectra of all the samples were recorded by using a spectrophotometer (PerkinElmer Lambda 950).

Conventional photoluminescence (PL) spectra were acquired at RT, using standard lock-in configuration, by exciting the samples with the 325-nm line of a He–Cd laser (with a power density of 100 W·cm^{-2}) and analyzed by a monochromator coupled to a GaAs photomultiplier tube (PMT). The up-conversion PL (UC-PL) measurements were performed using an EKSPLA PG122 optic parametric oscillator (OPO) with an output range of 420–2300 nm, which was pumped by the third harmonic of a Brilliant 5-ns-pulsed Nd:YAG laser (the resulting peak power density was about 10^9 W·cm^{-2}, for a spot diameter onto the sample of 100 μm). Using the OPO output at 980 nm, we were able to excite the $^4I_{11/2}$ and $^2F_{5/2}$ levels of Er^{3+} and Yb^{3+} ions, respectively. The high excitation power densities onto the samples allowed promoting up-conversion to higher energy levels in both RE species. The resulting luminescence spectra obtained in the visible range were acquired using a GaAs PMT. The excited PL study was carried out tuning the OPO output in the range from 950 to 1200 nm, while monitoring the 660 nm emission line of Er with a monochromator, corresponding to the transition of the up-converted energy level.

3. Results and discussion

Fig. 2 shows the XRD patterns of the three samples, before and after the annealing step. All samples were found to be polycrystalline and presented the highest intensity diffraction peak at around $2\theta = 34.4°$, indicating a hexagonal wurtzite structure with a strong preferred orientation along the [001] direction with the *c*-axis perpendicular to the substrate. Another weak peak from wurtzite structure was also observed at $2\theta = 47.67°$, corresponding to the reflection of (102) plane [18]. The annealed EZOA and EYZOA films showed the phases of Er_2O_3 and Yb_2O_3, respectively. In the case of EZOA, a peak of low intensity was observed at $2\theta = 29.31°$ that corresponds to the (222) reflection of Er_2O_3 cubic structure [19], and EYZOA showed a peak at $2\theta = 29.62°$, attributed to the (222) reflection of Yb_2O_3 [20]. The as-

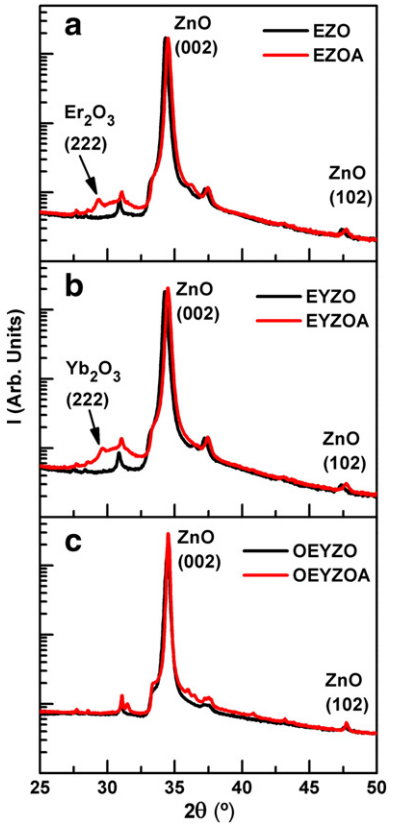

Fig. 2. XRD patterns plotted on a logarithmic scale of the as-deposited and annealed films: (a) EZO and EZOA, (b) EYZO and EYZOA, and (c) OEYZO and OEYZOA. The peaks that appear in all samples at $2\theta = 31.05°$ and $2\theta = 37.42°$ correspond to instrumental artifacts.

Please cite this article as: M. Lluscà, et al., Up-conversion effect of Er- and Yb-doped ZnO thin films, Thin Solid Films (2014), http://dx.doi.org/10.1016/j.tsf.2014.03.078

deposited layers did not present any feature related to the Er_2O_3 or Yb_2O_3 phases, suggesting that Er and/or Yb atoms are either substitutionally replacing Zn in the ZnO lattice or segregated to the non-crystalline region in grain boundaries. On the other hand, when the samples were annealed, the micro-structure of the films was changed by the plausible oxidation of Er and/or Yb and presented Er_2O_3 or Yb_2O_3 phases in the XRD patterns (the annealing process was done in an air atmosphere). The presence of Er_2O_3 or Yb_2O_3 phases was not observed in the OEYZO sample, associated either to the relatively small amount of Er and/or Yb atoms incorporated into the film (low doping level), or due to the absence of those phases for the employed deposition conditions. In fact, XPS analysis (see results and comments below) indicates an Er and Yb concentration of about 3% for samples EZOA and EYZOA and a very low concentration for sample OEYZOA (below the detection limit of our instrument), which could explain why Er_2O_3 phase has not been observed in the diffraction pattern of EYZOA. It is worth noticing that the peaks that were observed in all samples at $2\theta = 31.05°$ and $2\theta = 37.42°$ correspond to instrumental artifacts.

The lattice parameter value of each sample as well as that of undoped ZnO (ZO) grown under the same conditions with that of EZO and EYZO, have been estimated from the diffraction peaks related to the ZnO wurtzite structure (see Table 1). All as-deposited films showed c parameter values slightly higher than that of stress-free ZnO powder specimen ($c = 0.521$ nm, $a = 0.325$ nm) [18], indicating that the unit cells are elongated along the c-axis and the compressive forces were predominant as usual in RF sputtered ZnO thin films [21–23]. The internal compressive stress in the as-deposited films is assigned to the bombardment of energetic particles during deposition and not to the thermal stress originating from the difference between the thermal expansion coefficients of the film and the substrate. Even though, this thermal stress effect is slightly appreciable in the case of OEYZO where the film was deposited at 350 °C and the Corning glass gave a tensile stress to the film when it cooled down [24] compensating the compressive stress and giving a c value closer to the ideal from ZnO powder.

After the annealing, the peaks were shifted to higher diffraction angles and all the films showed lattice parameters (a and c) slightly lower than the ideal values for undoped ZnO powder. This suggested that the stress was changing from compressive to tensile. Although the post-annealing has been reported to contribute to the relaxation of RF sputtered ZnO films [25], it is possible that such high temperature of 800 °C produced tensile stress due to the mismatch between thermal energy coefficients when the films cooled down.

It was also observed that the annealing treatment did not produce any variation in the intensity of the main diffraction peak ($2\theta = 34.4°$) for EZO films, whereas that corresponding to EYZO and OEYZO films showed an increase in its intensity, which unequivocally indicates an enhancement of the film crystalline arrangement. The average crystallite size in the direction normal to the reflecting planes was not affected by the heat treatment except in the case of OEYZO and ZO, where it increased significantly after the annealing process. Actually, both films with almost no doping (OEYZO) or undoped (ZO) could present fewer grain boundaries due to the absence of RE ions at the grain boundaries and the annealing might have helped the grains to grow much bigger, since high temperature annealing stimulates the migration of grain boundaries and causes the coalescence of more grains suggesting that the Ostwald ripening process was also taking place.

Table 1
Average crystallite size in the direction normal to the reflecting plane and lattice parameter values obtained from XRD measurements of all samples and comparison with undoped ZnO before (ZO) and after the annealing treatment (ZOA). Standard lattice parameter values for ZnO, $c = 0.521$ nm and $a = 0.325$ nm [18].

Sample name	<D> (nm)	c (nm)	a (nm)
EZO	35	0.5220	0.3261
EZOA	34	0.5193	0.3233
EYZO	31	0.5226	0.3264
EYZOA	32	0.5195	0.3232
OEYZO	36	0.5202	0.3234
OEYZOA	54	0.5192	0.3221
ZO	21	0.5235	[a]
ZOA	50	0.5196	0.3201

[a] The peak corresponding to the (102) plane reflection did not appear in ZO diffraction pattern.

The composition of the films before and after the annealing was estimated from the XPS spectra and appeared to be invariable after the heat treatment (within the resolution provided by the system for such low concentrations). Table 2 presents the atomic concentration of Er and/or Yb incorporated to the films depending on the sputtering conditions and the number of pellets. Fig. 3 shows the XPS spectra of O 1*s* core level in the films, before and after annealing. To further study the bonding state of Zn, O and the doping elements in the ZnO films, a high resolution scan of O 1*s* peak was performed. From previous reports [26], O 1*s* state can be fitted into three Gaussian functions centered at ~529.9 eV, ~531.4 eV and ~532 eV. The peak at the lowest binding energy (BE) is associated with the O^{2-} ions at the intrinsic sites in the wurtzite structure; in other words, it indicates the presence of O bonds to Zn atoms or to substitutional Er^{3+} or Yb^{3+} ions in the ZnO matrix. The medium centered peak is attributed to the O^{2-} ions in the oxygen-deficient regions and the change in its intensity may be related to the variation of the concentration of oxygen vacancies. The peak at the highest BE position is usually attributed to chemisorbed oxygen species (that appears also in ZnO-based thin films without Er or Yb) [27,28] and/or to the formation of Er or Yb oxide [29,30]. Although the film surface was previously sputtered for 3 min, it does not strictly mean that the contamination component was completely removed [27,31].

As seen in Fig. 3, the intensity of the medium BE peak is always higher than the other peaks, indicating a large concentration of oxygen vacancies in the surface layers. The medium BE peak intensity at ~531.4 eV was found to decrease after the post-annealing process in the case of EZO and EYZO samples. This is reasonable due to the fact that EZO and EYZO films were deposited at room temperature with a lower oxygen concentration. For EZO and EYZO samples, the post-annealing process caused a slight increase of the higher BE peak, suggesting the formation of Er and Yb oxides and/or an increase of the surface contamination (chemisorbed oxygen species). To sum up, observing Er ^4d peak in EZO (not shown here) a small change in the peak shape was detected after annealing, presenting an increase in the contribution of Er_2O_3 on the area of the peak. This behavior is consistent with XRD results, where an Er_2O_3 phase was seen after annealing the sample. On the other hand, Yb_2O_3 contribution was not observed in Yb ^4d peak of EYZOA. In contrast, for OEYZO, the highest BE peak decreased after the annealing. Finally, and according to XRD results, the crystalline arrangement was enhanced by the annealing for EYZO and OEYZO samples. This result agrees with the behavior of the low BE peak, which also increased, indicating the formation of a larger number of bonds between Zn or the substitutional RE ions to O within the ZnO matrix.

All films were found to be transparent and showed integrated transmittance values above 80% within the range of 400 nm–1100 nm. In Fig. 4, the RT PL spectra obtained from the samples under study are displayed. Although PL measurements are extremely sensitive to laser focus and incidence angle, all measurements were carried in identical

Table 2
Atomic concentration of Er and Yb on the films, estimated from the XPS data analysis.

Sample name	Number of Er_2O_3 pellets	Number of Yb_2O_3 pellets	Atomic concentration
EZO	3	–	Er ~ 3%
EYZO	1	3	Er ~ 1%, Yb ~ 3%
OEYZO	1	3	Er < 1%, Yb < 1%

Please cite this article as: M. Lluscà, et al., Up-conversion effect of Er- and Yb-doped ZnO thin films, Thin Solid Films (2014), http://dx.doi.org/10.1016/j.tsf.2014.03.078

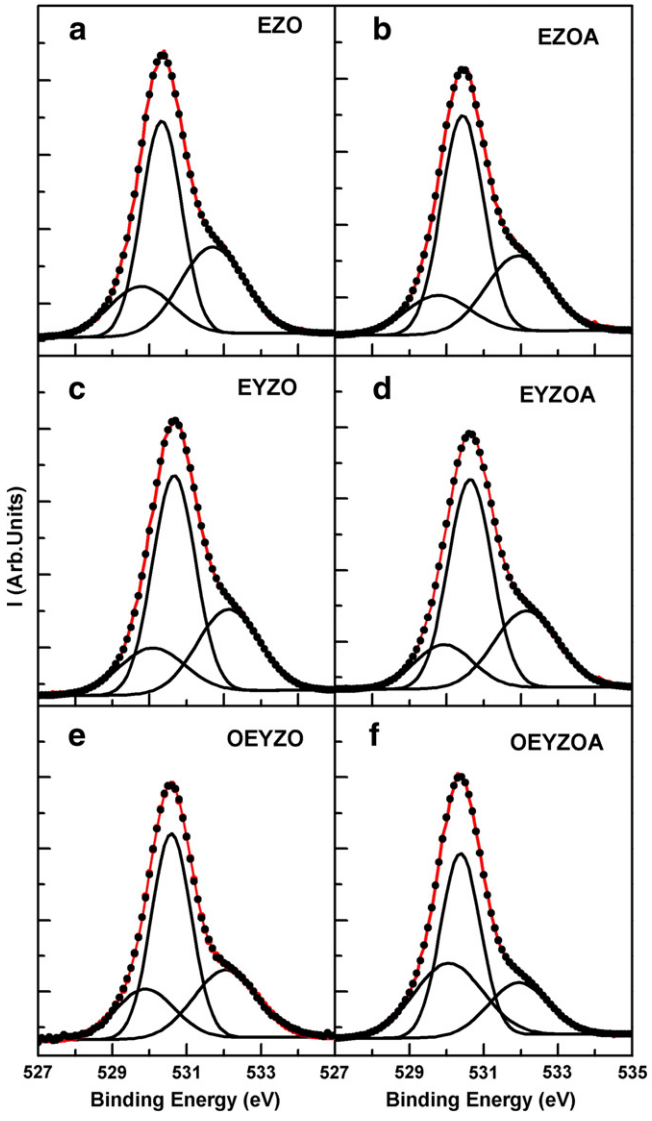

Fig. 3. XPS O 1*s* peak Gaussian deconvolution for (a) EZO, (b) EZOA, (c) EYZO, (d) EYZOA, (e) OEYZO and (f) OEYZOA. Black points indicate XPS spectra and red line represents the fitted function. (For interpretation of the references to color in this figure legend, the reader is referred to the web version of this article.)

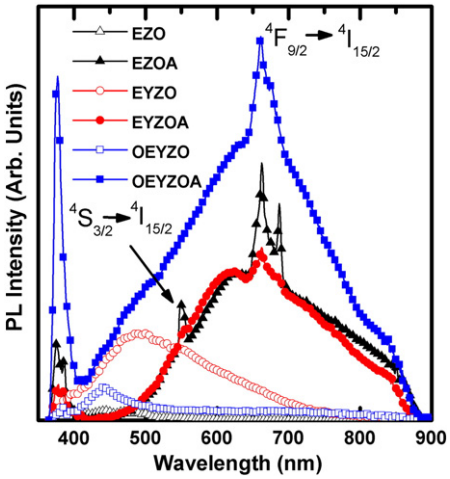

Fig. 4. RT PL spectra of the different samples considered for the present study. The 325-nm line from a He–Cd laser was employed to excite the samples, being the PL emission acquired in the near-UV and visible ranges. Open symbols indicate as-deposited samples, whereas full symbols account for the annealed ones. (For interpretation of the references to color in this figure, the reader is referred to the web version of this article.)

conditions, so that the relative intensity between the different spectra is directly comparable. The first main observation is the fact that as-deposited samples presented a broad band peaking around 450–500 nm, whereas annealed samples presented a spectrum typical from ZnO: a sharp emission around 375 nm and a broad band centered at 600–660 nm. The emission observed in the as-deposited samples is attributed to a combination of emissions coming from highly defective ZnO and the defects present in the Corning glass substrate (low intensity emission in the blue range).

As far as the annealed samples are concerned, the intensity of the emission at 375 nm, related to the excitonic band-to-band recombination (BBR) of ZnO (usually observed in the nanostructured material) [32], increased with the crystalline domain size, obtaining higher intensity for the sample deposited under O_2 atmosphere (see experimental results of XRD data). On the other hand, the broad visible emission (BVE) that these samples presented is due to the radiative recombination in deep-level defects such as oxygen vacancies and/or Zn atoms in interstitial position inside the ZnO lattice [33]. Considering the ratio between the maximum PL intensity of the BBR ($\lambda = 375$ nm) and BVE ($\lambda = 600$–660 nm, depending on the spectrum) bands, $r = I(\lambda_{BBR}) / I(\lambda_{BVE})$, we obtained a value of $r = 1.2$ for the annealed OEYZOA sample, that clearly overcomes those for EZOA and EYZOA samples ($r = 0.52$ and 0.22, respectively). One possible explanation is the higher stoichiometry and crystalline arrangement that this sample presents, as the deposition parameters and annealing process introduced a higher amount of O atoms to the ZnO matrix that contribute to reduce structural defects, reducing non-radiative paths and, in turn, enhancing the PL emission of ZnO. In addition, the three annealed samples presented peak-like emissions around 550 nm and 660–680 nm [34], related to radiative transitions between different electronic levels of Er^{3+} ions (see Fig. 1). This fact indicates that the Er^{3+} ions occupy optically active centers, either in the ZnO host (Er^{3+} ions are excited through the ZnO host matrix) or in grain boundaries [16]. Considering now the intensity dependence of the Er emission in annealed samples with and without Yb^{3+} ions (red full circles and black full triangles, respectively), a clear intensity reduction was observed for the samples containing Yb^{3+}. This fact could be associated with the lower Er content present in these samples (about one order of magnitude lower in composition, see Table 2). Therefore, this RE-related emission is comparable for all the annealed samples when using the host ZnO material to excite them, suggesting that the RE ions are well integrated inside the ZnO matrix. The active movements of O_2 during the annealing process result in an adequate environment of Er atoms forming an appropriate crystal configuration for the intra-4*f* shell transition where Er atoms are surrounded by O forming ErO_6 clusters [14–16].

The UC-PL spectra were obtained by exciting the samples using a single excitation wavelength in the range from 900 to 1300 nm and acquiring the emission in the range from 400 to 850 nm, i.e. at higher energies. We found that the excitation at 980 nm induced the optimum up-conversion emission at 660 nm; therefore, this wavelength was selected for exciting the samples in up-conversion experiments. The resulting UC-PL spectra are shown in Fig. 5(a). An intense emission can be appreciated around 660 nm that is composed by two different contributions, one centered at 655 and another at 675 nm [35] that we assign tentatively to a level splitting of the $^4F_{9/2}$ energy state of Er^{3+} ions. Both emissions present an energy value higher than the energy of the excitation photons, which clearly demonstrates that an up-conversion process is taking place in the Er^{3+} ions. Actually, the 980 nm excitation coincides in energy with the $^4I_{15/2} \rightarrow {}^4I_{11/2}$ transition, so that electrons initially in the ground state populate the excited $^4I_{11/2}$ level. The further absorption of photons from the excitation source may promote electrons in the latter state to higher energy ones, being $^4F_{7/2}$ the most probable one. This is called a two-photon absorption process,

Please cite this article as: M. Lluscà, et al., Up-conversion effect of Er- and Yb-doped ZnO thin films, Thin Solid Films (2014), http://dx.doi.org/10.1016/j.tsf.2014.03.078

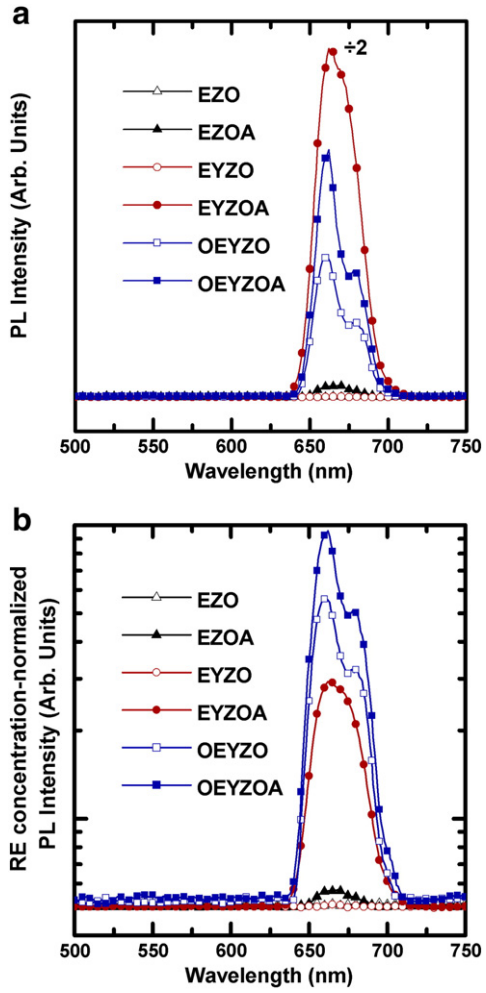

Fig. 5. (a) Up-conversion PL spectra of the samples under study. 980 nm was selected as the excitation wavelength, and resulting PL spectra were acquired through the visible range. The observed peaks belong to the $^4F_{9/2} \rightarrow {}^4I_{15/2}$ Er transition. (b) Up-conversion spectra displayed in (a), corrected taking into account the total rare-earth (Er and Yb) atomic concentration for each sample. Open symbols indicate as-deposited samples, whereas full symbols account for the annealed ones. (For interpretation of the references to color in this figure, the reader is referred to the web version of this article.)

and requires that the time interval between the arrivals of the involved photons is lower than the relaxation time of the intermediate energy level ($^4I_{11/2}$). The relaxation of the final high energy levels populates the $^4F_{9/2}$ electronic state, whose radiative decay towards the ground state originates the observed PL emission around 660 nm. Up-conversion emission corresponding to the $^4S_{3/2}$ decay has been observed by many other authors in similar material systems [36,37]; however, the lower Er concentration employed in our work, as well as the quality of the matrix surrounding the RE ions, may influence the transition probability between further separated energy states.

As can be observed in Fig. 5(a), the as-deposited samples either Er doped or Er–Yb co-doped did not show up-conversion emission, in agreement with the absence of RE-emission in conventional PL. On the other hand, if we compare the emission of these two samples after the annealing process, we observe an increase in the UC-PL due to the presence of Yb in the samples [see red full circles and black full triangles in Fig. 5(a)]. Actually, the $Er^{3+}{}^4I_{15/2} \rightarrow {}^4I_{11/2}$ transition (980 nm) presents exactly the same energy than (i.e. it is resonant with) the $^2F_{5/2} \rightarrow {}^2F_{7/2}$ one in Yb^{3+}. Consequently, the laser excitation of the sample not only populates the Er $^4I_{11/2}$ level but also the analogous one in Yb. Then, by means of direct transfer involving those states from different ionic species, the Er excited level substantially increases its population density. In addition, the relaxation of Yb^{3+} ions releases photons with the same energy than the incoming radiation, which in turn can activate the $^4I_{11/2} \rightarrow {}^4F_{7/2}$ transition in Er [38,39]. The sum of both possible pictures results in an enhancement of the up-conversion probability in Er^{3+} ions, as demonstrated by the increase of about one order of magnitude in the UC-PL of the sample containing Yb^{3+} ions.

The UC-PL emission of the samples deposited under an O_2 atmosphere presented a different behavior: both the as-deposited (OEYZO) and annealed (OEYZOA) samples displayed a strong emission, but lower than the EYZOA sample. The fact that as-deposited samples present UC-PL signal may account for the oxygen-rich atmosphere and substrate temperature employed during deposition (350 °C); this temperature seems high enough for activating the RE ions but not the ZnO matrix, as no conventional PL signal was observed (see Fig. 4). In order to compare the emission of these samples to the previous ones, we have normalized the spectra to the concentration of the different involved RE atoms (Er and Yb). Although the emission only comes from Er, the normalization also took into account the Yb concentration, as both species are excited with the incoming radiation at 980 nm. The normalized spectra are displayed in Fig. 5(b). It is clearly observed that, under equivalent ion concentration conditions, samples that were deposited under O_2 flow show a stronger emission, even in the as-deposited case. As mentioned in the conventional PL analysis, the extra O atoms occupy O vacancies within the lattice, thus increasing the crystalline domain size. Moreover, XRD verified that these crystalline domains undergo a clear hydrostatic compression (ZnO lattice parameters were reduced in 0.002–0.003 nm). With these facts, we assume that the confinement of the RE ions within the matrix, and thus their localization, is strongly increased; therefore, the probability of the resonant transfer mechanism to occur (from Yb^{3+} to Er^{3+} ions) is enhanced.

In conclusion, these results indicate that Er–Yb co-doped ZnO deposited in O-rich atmosphere and at high temperatures can be used as up-conversion system to take profit of the near infrared light. Probably ErO_6 clusters are formed either at the grain boundaries or within the ZnO matrix.

4. Conclusion

Er doped and Er and Yb co-doped thin ZnO films were deposited by RF magnetron sputtering, and annealed at 800 °C to optically activate Er^{3+} ions. All the films showed a (002) preferential orientation with the *c*-axis perpendicular to the substrate surface. Er_2O_3 and Yb_2O_3 phases were observed on Er and Yb co-doped films after the annealing. XPS results showed that Er and Yb atoms were incorporated to the ZnO films. For EZO and EYZO samples, the analysis of the O 1*s* peak presented an increase of the highest BE peak after the annealing treatment, suggesting the formation of RE oxides according to XRD results. The annealing treatment appeared to be essential to convert Er^{3+} ions in optically active centers, whose PL emission is due to an energy transfer from the matrix when exciting with UV laser radiation. Moreover, UC-PL was observed, probably arising from a two-photon absorption mechanism of IR photons in Er^{3+} ions, which afterwards produce a higher energy photon in the visible range. The presence of Yb^{3+} ions clearly enhanced the up-conversion emission by direct transfer from the $^2F_{5/2}$ Yb excited level to the $^4I_{11/2}$ Er one. Both treatments, air post-annealing, and deposition in O_2 flow while annealing the substrate seem to be suitable mechanisms to produce ErO_6 clusters either in the ZnO matrix or at grain boundaries.

Acknowledgments

This work has been supported by the Spanish Ministerio de Economía y Competitividad and the European Regional Development Fund through the projects AMIC (ENE2010-21384-C04-03), LEOMIS (TEC2012-38540-C02-01) and INNDISOL (IPT-420000-2010-6).

References

[1] B.M. van der Ende, L. Aarts, A. Meijerink, Lanthanide ions as spectral converters for solar cells, Phys. Chem. Chem. Phys. 11 (2009) 11081.
[2] H.Q. Wang, M. Batentschuk, A. Osvet, L. Pinna, C.J. Brabec, Rare-earth ion doped up-conversion materials for photovoltaic applications, Adv. Mater. 23 (2011) 2675.
[3] C.W. Thiel, Y. Sun, R.L. Cone, Progress in relating rare-earth ion 4f and 5d energy levels to host bands in optical materials for hole burning, quantum information, and phosphors, J. Mod. Opt. 49 (2002) 2399.
[4] S.A. Hilderbrand, F. Shao, C. Salthouse, U. Mahmood, R. Weissleder, Upconverting luminescent nanomaterials: application to *in vivo* bioimaging, Chem. Commun. 28 (2009) 4188.
[5] X. Wang, X. Kong, Y. Yu, Y. Sun, H. Zhang, Effect of annealing on upconversion luminescence of ZnO:Er^{3+} nanocrystals and high thermal sensitivity, J. Phys. Chem. 111 (2007) 15119.
[6] X. Meng, C. Liu, F. Wu, J. Li, Strong up-conversion emissions in ZnO:Er^{3+}, ZnO:Er^{3+}–Yb^{3+} nanoparticles and their surface modified counterparts, J. Colloid Interface Sci. 358 (2011) 334.
[7] J.F. Philipps, T. Töpfer, D. Ehrt, R. Sauerbrey, Spectroscopic and lasing properties of Er^{3+}:Yb^{3+}-doped, Appl. Phys. B 405 (2001) 399.
[8] A.S. Oliveira, M.T. de Araujo, A.S. Gouveia-Neto, J.A. Medeiros Neto, A.S.B. Sombra, Y. Messaddeq, Frequency upconversion in Er^{3+}/Yb^{3+}-codoped chalcogenide glass, Appl. Phys. Lett. 72 (1998) 753.
[9] M. Wang, C. Mi, W. Wang, C. Liu, Y. Wu, Z. Xu, B. Mao, S. Xu, Immunolabeling and NIR-excited fluorescent imaging of HeLa cells by using $NaYF_4$:Yb,Er upconversion nanoparticles, ACS Nano 3 (2009) 1580.
[10] X. Orignac, D. Barbier, X. Min, R.M. Almeida, O. Mccarthy, E. Yeatman, Sol–gel silica/titania-on-silicon Er/Yb-doped waveguides for optical amplification at 1.5 μm, Opt. Mater. 12 (1999) 1.
[11] P. Pellegrino, B. Garrido, Y. Lebour, J.A. Moreno, C. Garcia, J.R. Morante, P. Bettotti, L. Pavesi, M. Prassas, Luminescent properties of Er and Si co-implanted silicates, Opt. Mater. 27 (2005) 910.
[12] D. Navarro-Urrios, M. Melchiorri, N. Daldosso, L. Pavesi, C. García, P. Pellegrino, B. Garrido, G. Pucker, F. Gourbilleau, R. Rizk, Optical losses and gain in silicon-rich silica waveguides containing Er ions, J. Lumin. 121 (2006) 249.
[13] C. Klingshirn, ZnO: from basics towards applications, Phys. Status Solidi B 244 (2007) 3027.
[14] M. Ishii, S. Komuro, T. Morikawa, Y. Aoyagi, Local structure analysis of an optically active center in Er-doped ZnO thin film, J. Appl. Phys. 89 (2001) 61.
[15] L. Douglas, R. Mundle, R. Konda, C.E. Bonner, A.K. Pradhan, D.R. Sahu, J.-L. Huang, Influence of doping rate in films on emission characteristics, Opt. Lett. 33 (2008) 815.
[16] Z. Zhou, T. Komaki, A. Koizumi, T. Komori, M. Yoshino, M. Morinaga, Y. Fujiwara, Y. Takeda, Effects of nitrogen irradiation on photoluminescence around 1.54 μm from Er-containing ZnO, Mater. Trans. 45 (2004) 2003.
[17] E.J. Mittemeijer, U. Welzel, The "state of the art" of the diffraction analysis of crystallite size and lattice strain, Z. Kristallogr. 223 (2008) 552.
[18] JCPDS card No 36-1451.
[19] JCPDS card No 8-0050.
[20] JCPDS card No 41-11506.
[21] W.L. Dang, Y.Q. Fu, J.K. Luo, A.J. Flewitt, W.I. Milne, Deposition and characterization of sputtered ZnO films, Superlattice. Microst. 42 (2007) 89.
[22] R. Ondo-Ndong, G. Ferblantier, M. Al Kalfioui, A. Boyer, A. Foucaran, Properties of RF magnetron sputtered zinc oxide thin films, J. Cryst. Growth 255 (2003) 130.
[23] J.H. Jou, M.Y. Han, D.J. Cheng, Substrate dependent internal stress in sputtered zinc oxide thin films, J. Appl. Phys. 71 (1992) 4333.
[24] S.Y. Hua, Y.C. Lee, J.W. Lee, J.C. Huang, J.L. Shen, W. Water, The structural and optical properties of ZnO/Si thin films by RTA treatments, Appl. Surf. Sci. 254 (2008) 1578.
[25] E.M. Bachari, G. Baud, S.B. Amor, M. Jacquet, Structural and optical properties of sputtered ZnO films, Thin Solid Films 348 (1999) 165.
[26] Y. Chen, X.L. Xu, Effect of oxygen deficiency on optical band gap shift in Er-doped ZnO thin films, Physica B 406 (2011) 3121.
[27] M.N. Islam, T.B. Ghosh, K.L. Chopra, H.N. Acharya, XPS and X-ray diffraction studies of aluminum-doped zinc oxide transparent conducting films, Thin Solid Films 280 (1996) 20.
[28] H.T. Cao, Z.L. Pei, J. Gong, C. Sun, R.F. Huang, L.S. Wen, Preparation and characterization of Al and Mn doped ZnO (ZnO: (Al, Mn)) transparent conducting oxide films, J. Solid State Chem. 177 (2004) 1480.
[29] C. Liau, L. Chao, Growth and characterization of Er doped ZnO prepared by reactive ion beam sputtering, in: Paul K. Chu (Ed.), 2010 3rd International Nanoelectronics Conference, IEEE, Piscataway, N.J., 2010, p. 976.
[30] S. Komuro, T. Katsumata, T. Morikawa, X. Zhao, H. Isshiki, Y. Aoyagi, Highly erbium-doped zinc-oxide thin film prepared by laser ablation and its 1.54 μm emission dynamics, J. Appl. Phys. 88 (2000) 7129.
[31] M. Chen, X. Wang, Y. Yu, Z. Pei, X. Bai, C. Sun, R. Huang, L. Wen, X-ray photoelectron spectroscopy and Auger electron spectroscopy studies of Al-doped ZnO films, Appl. Surf. Sci. 158 (2000) 134.
[32] Y.X. Liu, Y.C. Liu, C.L. Shao, R. Mu, Excitonic properties of ZnO nanocrystalline films prepared by oxidation of zinc-implanted silica, J. Phys. D. Appl. Phys. 37 (2004) 3025.
[33] Y. Chen, D.M. Bagnall, H. Koh, K. Park, K. Hiraga, Z. Zhu, T. Yao, Plasma assisted molecular beam epitaxy of ZnO on c-plane sapphire: growth and characterization, J. Appl. Phys. 84 (1998) 3912.
[34] Z. Pan, S.H. Morgan, A. Ueda, R. Aga Jr., A. Steigerwald, A.B. Hmelo, R. Mu, Er-doped ZnO films grown by pulsed e-beam deposition, J. Phys. Condens. Matter 19 (2007) 266216.
[35] S. Hinojosa, O. Barbosa García, M.A. Meneses-Nava, J.L. Maldonado, E. de la Rosa Cruz, G. Ramos Ortiz, Luminescent properties and energy transfer processes of co-doped Yb–Er poly-crystalline YAG matrix, Opt. Mater. 27 (2005) 1839.
[36] F. Vetrone, J.C. Boyer, J.A. Capobianco, A. Speghini, M. Bettinelli, 980 nm excited upconversion in an Er-doped ZnO–TeO_2 glass, Appl. Phys. Lett. 80 (2002) 1752.
[37] A. Kanoun, N. Jaba, A. Brenier, Time-resolved up-converted luminescence in Er^{3+}-doped TeO_2–ZnO glass, Opt. Mater. 26 (2004) 79.
[38] L. Yang, X. Wang, Z. Li, P. Liu, F. Liu, S. Ge, F. Song, B. Liu, Y. Shi, R. Zhang, (Er, Yb)-co-doped multifunctional ZnO transparent hybrid materials: fabrication, luminescent and magnetic properties, J. Phys. D. Appl. Phys. 44 (2011) 155404.
[39] Y. Liu, Q. Yang, C. Xu, Single-narrow-band red upconversion fluorescence of ZnO nanocrystals codoped with Er and Yb and its achieving mechanism, J. Appl. Phys. 104 (2008) 064701.

Please cite this article as: M. Lluscà, et al., Up-conversion effect of Er- and Yb-doped ZnO thin films, Thin Solid Films (2014), http://dx.doi.org/10.1016/j.tsf.2014.03.078